

H1prelim-20-033

December 2020

Submitted to **Initial Stages 2021**, Israel, 10-15 January, 2021

Search for collectivity in e-p collisions with H1

H1 Collaboration

Abstract

Measurements of two- and multi-particle angular correlations in DIS and photoproduction ep collisions at $\sqrt{s} = 319$ GeV are presented as a function of charged-particle multiplicity. The data were collected using the H1 detector at HERA. Since no long-range ridge structure is observed in the correlation functions over the full multiplicity range, upper limits of ridge yield are provided as functions of particle multiplicity. The second-order ($V_{2\Delta}$) and third-order ($V_{3\Delta}$) azimuthal anisotropy Fourier harmonics of charged particles are extracted from long-range two-particle correlations as functions of particle multiplicity. The $C_2\{4\}$ signals are also extracted from four-particle correlations for the first time in ep collisions, which are positive or consistent with 0. These observations do not indicate the kind of collective behavior observed at the RHIC and LHC in high-multiplicity hadronic collisions.

1 Introduction

The observation of collective behavior in high final-state particle multiplicity proton-proton and proton-nucleus [1–4] collisions at RHIC and the LHC has opened up new opportunities for studying novel dynamics of particle production in small, high-density QCD systems. At present, it is unclear whether the collectivity observed in small systems originates from the hydrodynamic collective flow of a strongly interacting and expanding medium [5–7]. This motivates the search for collective behavior in ep collisions at the Hadron Electron Ring Accelerator (HERA).

A key feature of the observed collectivity in small system is an enhanced structure in the two-particle $\Delta\eta$ - $\Delta\phi$ correlation functions on the near side (relative azimuthal angle $|\Delta\phi| \approx 0$) extending over a wide range in relative pseudorapidity, known as the “ridge”. In hydrodynamic models, the detailed azimuthal correlation structure of emitted particles can be characterized by its Fourier components [8], in particular the second and third Fourier components, known as elliptic (v_2) and triangular (v_3) flow. Furthermore, collectivity can be probed more directly using the multi-particle correlations [9] since it is intrinsically a multi-particle phenomenon.

In this note, measurements of two- and multi-particle angular correlations in DIS and photo-production ep collisions at $\sqrt{s} = 319$ GeV are presented as a function of charged-particle multiplicity. The data were collected using the H1 detector at HERA. Since no long-range ridge structure is observed in the correlation functions over the full multiplicity range, upper limits of ridge yield are provided as functions of particle multiplicity. The second-order ($V_{2\Delta}$) and third-order ($V_{3\Delta}$) azimuthal anisotropy Fourier harmonics of charged particles are extracted from long-range two-particle correlations as functions of particle multiplicity. The $C_2\{4\}$ signals are also extracted from four-particle correlations for the first time in ep collisions, which are positive or consistent with 0. These observations do not indicate the kind of collective behavior observed at the RHIC and LHC in high-multiplicity hadronic collisions.

2 Event and Track Selections

The data used in this analysis was taken in H1 detector at Hera during 2006-2007. During this period, the Hera accelerator collided 27.6 GeV e^\pm beams with 920 GeV proton beams, which yields a nominal centre-of-mass energy of 319 GeV.

DIS events were recorded using triggers based on electromagnetic energy deposits in the SpaCal calorimeter. The scattered lepton, defined by the most energetic SpaCal cluster, is required to have an energy E_e larger than 12 GeV. The kinematic phase space is defined by $5 < Q^2 < 100$ GeV² and $0.0375 < y < 0.6$. In addition, x is required to be in the range of $0.0001 < x < 0.01$. Additional selections are made to reduce QED radiation effects and to suppress background events. The z coordinate of the event vertex is required to be within 35 cm of the nominal interaction point. Events with high energy initial state photon radiation are rejected by requiring $35 < \sum_i (E_i - p_{z,i}) < 75$ GeV.

The photo-production events were triggered by the signal of scattered electrons in electron tagger combining with a hardware track trigger with at least 1 track with $p_T > 0.9$ GeV. In order to ensure the track trigger having reliable efficiency, events are required to contain at least one reconstructed track with $p_T > 0.9$ GeV. Additional selections are applied on tagged position $x_{position}$, tagged electron energy E_e^{tagged} , and tagged photon energy E_γ^{tagged} . Namely $x_{position} + 0.4E_e^{tagged} > 0$, $-3.0 < x_{position} < 3.0$ and $E_e^{tagged} + E_\gamma^{tagged} < 20$ GeV. The z coordinate of the event vertex is required to be within 30 cm of the nominal interaction point.

Two types of tracks have been used in the analysis: the central track measured only in central tracking detectors (CJC - the central drift chamber, CST - a Central Silicon Track detector) and the combined tracks measured in central and forward trackers (FTD). In order to provide high efficiency of the track reconstruction, the following cuts are applied. For the central tracks:

- The transverse momentum $p_T > 0.07$ GeV.
- The distance of the closest approach of the track in the $r\phi$ plane to the primary vertex is required to be less than 2 cm.
- The starting point of a track is required to be within 50 cm from the center of the detector in the radial direction.
- The radial length L (the radial distance between the first and the last hit) is required to be larger than 10 (5) cm for tracks with polar angle $\theta \leq (>)150$ deg.

For the combined tracks:

- The transverse momentum $p_T > 0.12$ GeV.
- The momentum $p > 0.5$ GeV.
- The polar angle $10 \text{ deg} < \theta < 30 \text{ deg}$.
- The distance of the closest approach of the track in the $r\phi$ plane to the primary vertex is required to be less than 5 cm.
- The starting point of a track is required to be within 50 cm from the center of the detector in the radial direction.
- The χ^2 of vertex fit to be less than 50.

The charged particle multiplicity ($N_{\text{trk}}^{\text{obs}}$) is defined as the number of reconstructed tracks, after the selections, with $0.3 < p_T < 3.0$ GeV and $-1.6 < \eta < 1.6$. The tracks used for correlation studies are required to have $0.3 < p_T < 3.0$ GeV and $-1.6 < \eta < 1.6$ in photo-production events, while in DIS events additional requirement are applied in hadronic center-of-mass

(HCM) frame with $0.3 < p_T^{HCM} < 3.0$ GeV and $0 < \eta^{HCM} < 5$.

3 Analysis Technique

The construction of the two-particle correlation function follows the same procedure established in Refs. [1, 10–12]. The number of trigger particles (tracks passing selection) in the event is denoted by N_{trig} . Particle pairs are formed by associating each trigger particle with the remaining charged tracks. The two-dimensional (2D) correlation function is defined in the same way as in previous analyses as

$$\frac{1}{N_{\text{trig}}} \frac{d^2 N^{\text{pair}}}{d\Delta\eta d\Delta\phi} = B(0, 0) \times \frac{S(\Delta\eta, \Delta\phi)}{B(\Delta\eta, \Delta\phi)}, \quad (1)$$

where $\Delta\eta$ and $\Delta\phi$ are the differences in η and ϕ of the pair. The same-event pair distribution, $S(\Delta\eta, \Delta\phi)$, represents the yield of particle pairs normalized by N_{trig} from the same event,

$$S(\Delta\eta, \Delta\phi) = \frac{1}{N_{\text{trig}}} \frac{d^2 N^{\text{same}}}{d\Delta\eta d\Delta\phi}. \quad (2)$$

The mixed-event pair distribution,

$$B(\Delta\eta, \Delta\phi) = \frac{1}{N_{\text{trig}}} \frac{d^2 N^{\text{mix}}}{d\Delta\eta d\Delta\phi}, \quad (3)$$

is constructed by pairing the trigger particles in each event with the associated charged primary tracks from 5 different randomly selected events in the same 2 cm wide range of vertex position in the z direction and from the same multiplicity range. Here, N^{mix} denotes the number of pairs taken from the mixed events. The ratio $B(0, 0)/B(\Delta\eta, \Delta\phi)$ mainly accounts for the pair acceptance effects, with $B(0, 0)$ representing the mixed-event associated yield for both particles of the pair going in approximately the same direction and thus having maximum pair acceptance (with a bin width of 0.3 in $\Delta\eta$ and $\pi/16$ in $\Delta\phi$). Thus, the quantity in Eq. (1) is effectively the per-trigger-particle associated yield.

To further quantify the correlation structure, the 2-D distributions are reduced to one-dimensional (1-D) distributions in $\Delta\phi$ by averaging over the $\Delta\eta$ range [1, 10, 11, 13]. In the presence of multiple sources of correlations, the yield for the correlation of interest is commonly estimated using an implementation of the zero-yield-at-minimum (ZYAM) method [14]. A third-order Fourier series is first fitted to the 1-D $\Delta\phi$ correlation function in the region $0.1 < |\Delta\phi| < 2$. The minimum value of the fit is then subtracted from the correlation function as a constant background (containing no information of correlations) to shift its minimum to coincide with zero associated yield. Fig. 3 shows the 1-D $\Delta\phi$ correlation function and the fit for ZYAM in H1 DIS events with $15 \leq N_{\text{trk}}^{\text{obs}} < 20$ in the range of $1.5 < |\Delta\eta^{HCM}| < 2.0$, as well as the 1-D $\Delta\phi$ correlation function after ZYAM.

After ZYAM, an integral is performed in the range between 0 and the $\Delta\phi$ value where the ZYAM minimum is found to extract the ridge yield (Y_{ridge}). Since there is no ridge structure observed in either DIS or photo-production data, the integral values are consistent with 0 within uncertainties. Instead of reporting the ridge yield, limits are extracted using a bootstrap

procedure. Each data point of the 1-D $\Delta\phi$ correlation function is varied, independently, according to its statistical and systematic uncertainties (described later in this section) to form a new 1-D $\Delta\phi$ correlation function. The ridge yield is then extracted from the new 1-D $\Delta\phi$ correlation function. The procedure is carried out 2.5 million times where a distribution of ridge yield is obtained. The distributions are fitted by Gaussian functions where the mean ± 2 sigma of the Gaussian fit represents the 95% confidence level limits of the ridge yield. Fig. 4 shows the distribution of the ridge yield from bootstrap in DIS events with $15 \leq N_{\text{trk}}^{\text{obs}} < 20$ in the range of $1.5 < |\Delta\eta^{\text{HCM}}| < 2.0$.

Azimuthal anisotropy harmonics of charged particles are extracted via a Fourier decomposition of $\Delta\phi$ correlation functions averaged over $1.5 < |\Delta\eta| < 2.0$ and $2.0 < |\Delta\eta| < 3.0$,

$$\frac{1}{N_{\text{trig}}} \frac{dN^{\text{pair}}}{d\Delta\phi} = \frac{N_{\text{assoc}}}{2\pi} \left[1 + \sum_n 2V_{n\Delta} \cos(n\Delta\phi) \right], \quad (4)$$

as was done in Refs. [1, 10–12]. Here, $V_{n\Delta}$ are the Fourier coefficients and N_{assoc} represents the total number of pairs per trigger particle. The first five Fourier terms are included in the fits to the correlation functions. Including additional terms has a negligible effect on the results of the Fourier fit.

To further explore the possible collective nature of the long-range correlations, a four-particle cumulant analysis is used to extract the $C_2\{4\}$ with the standard cumulant method, the 2 subevent method and the 3 subevent method following the procedure in Ref. [9].

In order to determine acceptance and efficiency, the DIS process is simulated by different Monte Carlo (MC) event generators, which include the hard scattering process and simulation of higher order QCD correction in form of parton shower and hadronisation. Brief descriptions of the MC generators are given below:

- The **RAPGAP 3.1** [15] MC event generator matches first order QCD matrix elements to the Dokshitzer-Gribov-Lipatov-Altarelli-Parisi (DGLAP) [16–19] parton showers with strongly ordered transverse momenta of subsequently emitted partons. The factorisation and renormalisation scales are set to $\mu_f = \mu_r = \sqrt{Q^2 + \hat{p}_T^2}$, where \hat{p}_T is the transverse momentum of the outgoing hard parton from the matrix element in the center-of-mass frame of the hard subsystem. The CTEQ 6L [20] leading order parametrisation of the parton density function (PDF) is used.
- The **DJANGO 1.4** [21] MC event generator used the Color Dipole Model (CDM) as implemented in ARIADNE [22], which models first order QCD processes and creates dipoles between colored partons. Gluon emission is treated as radiation from these dipoles, and new dipoles are formed from the emitted gluons from which further radiation is possible. The radiation pattern of the dipoles includes interference effects, thus modelling gluon coherence. The transverse momenta of the emitted partons are not ordered in transverse momentum with respect to rapidity, producing a configuration similar to the Balitsky-Fadin-Kuraev-Lipatov (BFKL) [23–25] treatment of parton evolution [26]. The CTEQ 6L [20] at leading order is used as the PDF.

The generated events are passed through a detailed simulation of the H1 detector response based on the GEANT3 simulation program [27] and are processed using the same reconstruction and analysis chain as used for the data. For the determination of the detector effects both the RAPGAP and DJANGO predictions are studied. Fig. 7 and 8 show examples of 1D $\Delta\phi^{\text{HCM}}$ correlation functions from RAPGAP and DJANGO simulations, respectively.

Fig. 9 and 11 show $V_{2\Delta}$, $V_{3\Delta}$ and $C_2\{4\}$ from the two event generators. The measurements from RAPGAP agree better with the results from H1 data than those from DJANGO. Therefore, the detector corrections determined from RAPGAP simulation are applied to the results, while the difference between corrections from RAPGAP and DJANGO are quoted as systematic uncertainties. On the other hand, no corrections from MC studies has been applied to the photoproduction results. In addition to the systematic uncertainties from MC dependence, other systematic uncertainty are also considered:

- **Track charge.** The positive and negative charged particles can have slightly different acceptance and efficiency. The results from positive and negative charged particles are compared for the systematic uncertainty studies.
- **Vertex position.** Events with different vertex z position can have slightly different acceptance and efficiency. The results from $vtx_z < 0$ and $vtx_z > 0$ are compared for the systematic uncertainty studies.

4 Results

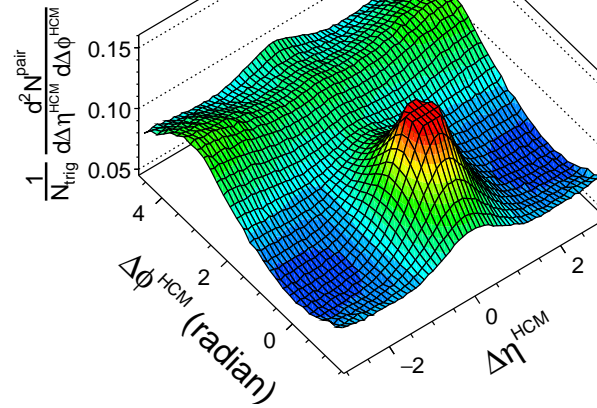
H1 Preliminary

ep $\sqrt{s} = 319$ GeV

$5 < Q^2 < 100$ GeV²

$2 \leq N_{\text{trk}}^{\text{obs}} < 4$

$0.3 < p_{\text{T}}^{\text{HCM}} < 3.0$ GeV



H1 Preliminary

ep $\sqrt{s} = 319$ GeV

$5 < Q^2 < 100$ GeV²

$15 \leq N_{\text{trk}}^{\text{obs}} < 20$

$0.3 < p_{\text{T}}^{\text{HCM}} < 3.0$ GeV

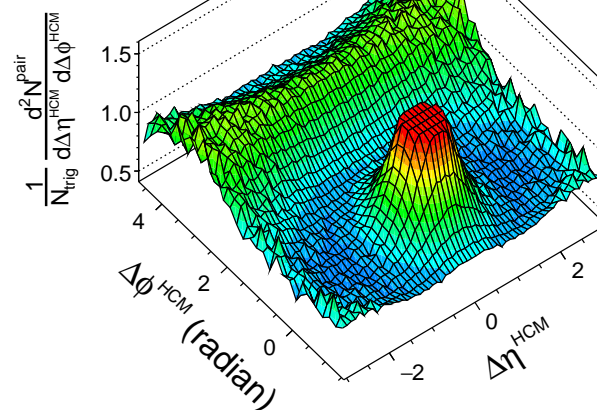


Figure 1: Two particle correlation functions in H1 DIS events with $2 \leq N_{\text{trk}}^{\text{obs}} < 4$ and $15 \leq N_{\text{trk}}^{\text{obs}} < 20$ for charged particles with $0.3 < p_{\text{T}}^{\text{HCM}} < 3.0$ GeV

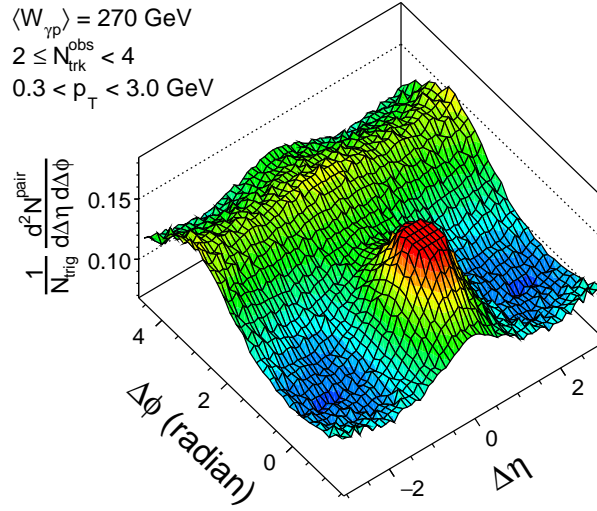
H1 Preliminary

ep photoproduction

$\langle W_{\gamma p} \rangle = 270$ GeV

$2 \leq N_{\text{trk}}^{\text{obs}} < 4$

$0.3 < p_{\text{T}} < 3.0$ GeV



H1 Preliminary

ep photoproduction

$\langle W_{\gamma p} \rangle = 270$ GeV

$15 \leq N_{\text{trk}}^{\text{obs}} < 20$

$0.3 < p_{\text{T}} < 3.0$ GeV

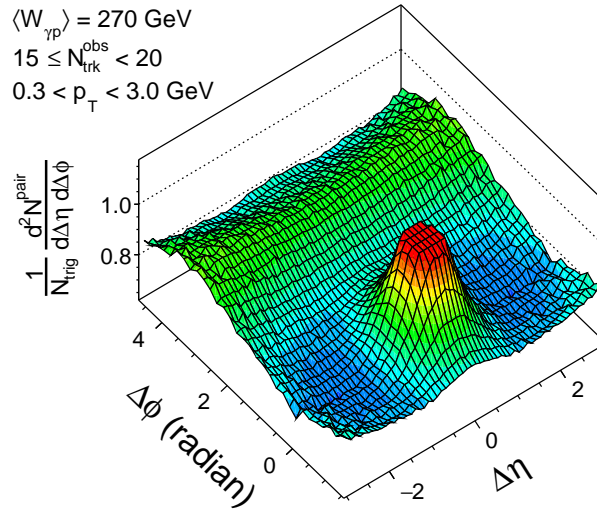


Figure 2: Two particle correlation functions in H1 photo-production events with $2 \leq N_{\text{trk}}^{\text{obs}} < 4$ and $15 \leq N_{\text{trk}}^{\text{obs}} < 20$ for charged particles with $0.3 < p_{\text{T}} < 3.0$ GeV

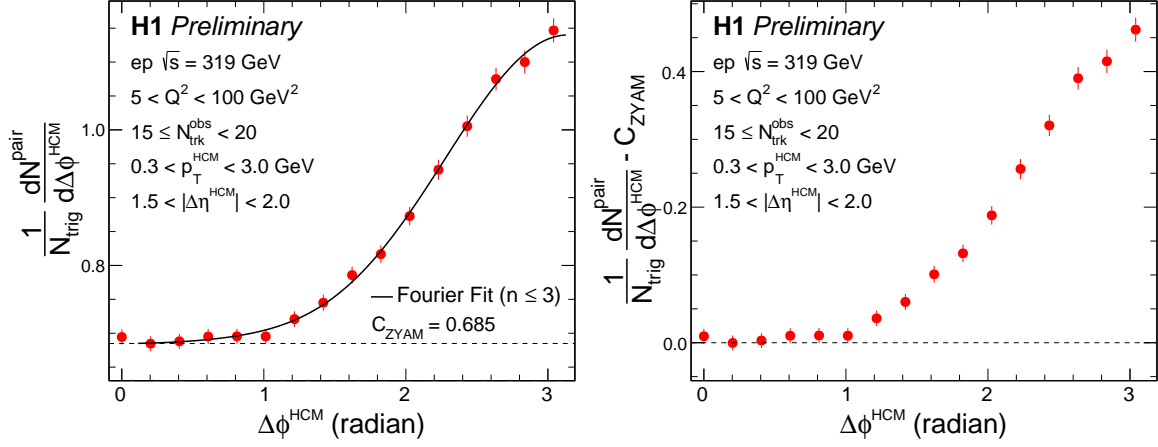


Figure 3: 1D $\Delta\phi^{\text{HCM}}$ correlation functions with $1.5 < |\Delta\eta^{\text{HCM}}| < 2.0$ in H1 DIS events with $15 \leq N_{\text{trk}}^{\text{obs}} < 20$ for charged particles with $0.3 < p_{\text{T}}^{\text{HCM}} < 3.0$ GeV, before (left) and after (right) ZYAM procedure.

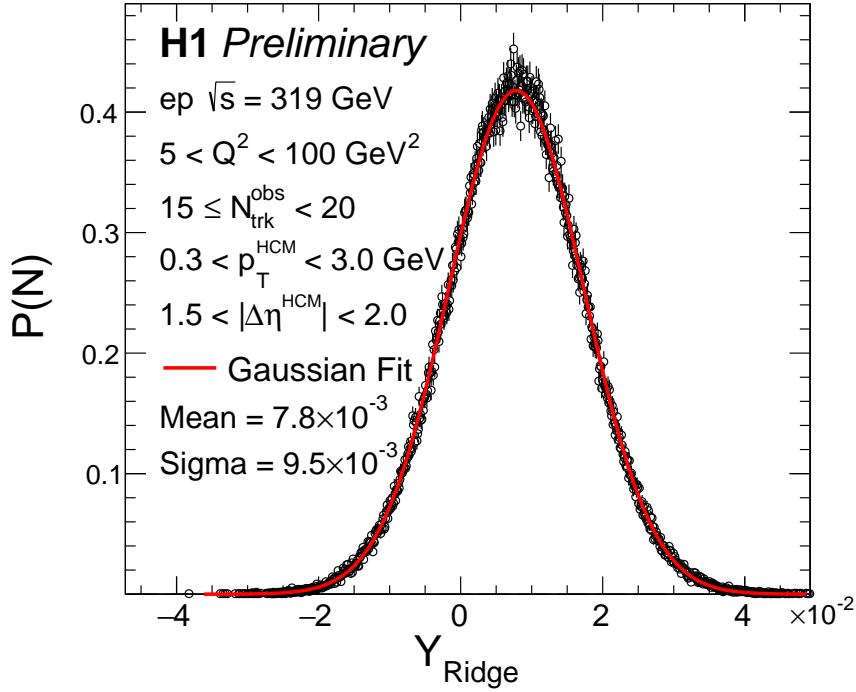


Figure 4: Ridge yield distribution from bootstrap in H1 DIS events with $15 \leq N_{\text{trk}}^{\text{obs}} < 20$ for charged particles with $0.3 < p_{\text{T}}^{\text{HCM}} < 3.0$ GeV and $1.5 < |\Delta\eta^{\text{HCM}}| < 2.0$. The data is fit by a Gaussian function to extract mean and sigma.

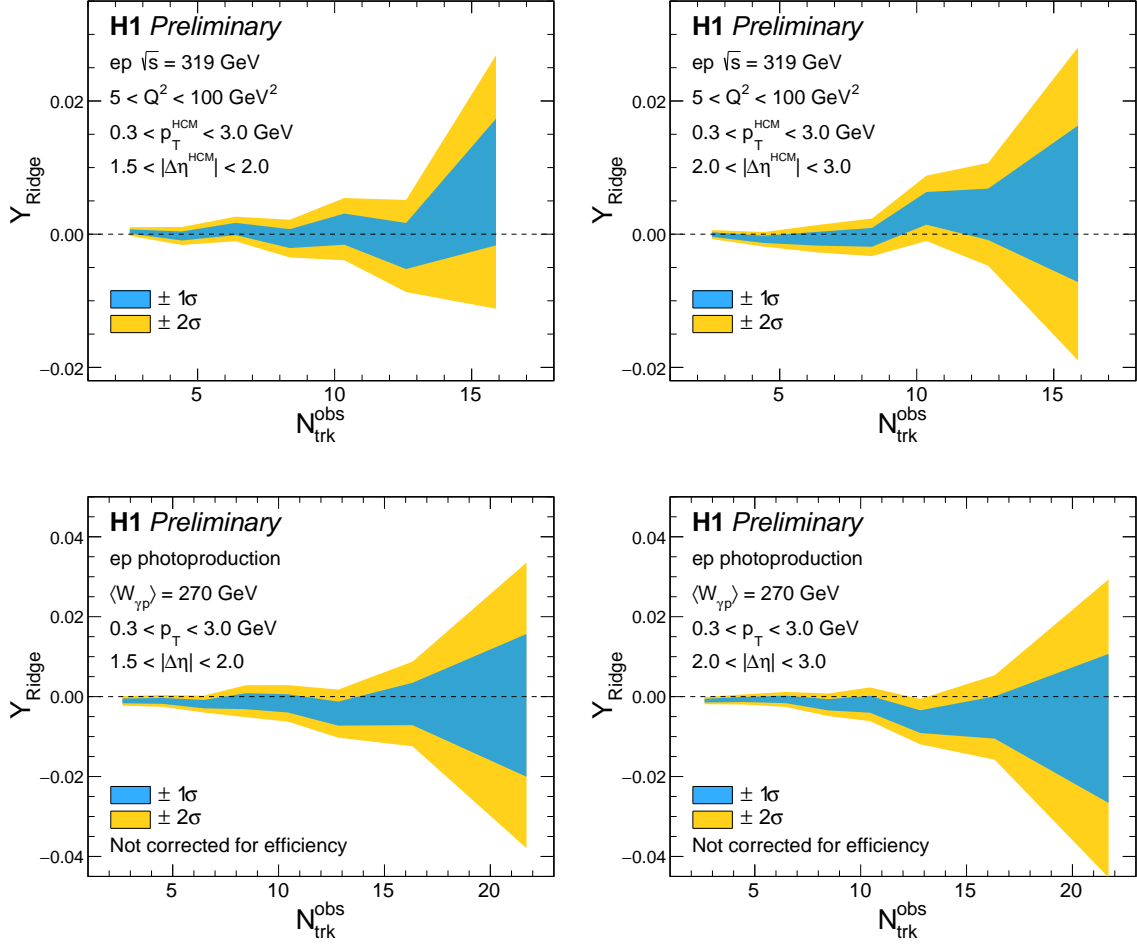


Figure 5: 1 and 2 sigma ridge yield limit from bootstrap as function of multiplicity in H1 DIS (top) and photo-production (bottom) events for $1.5 < |\Delta\eta| < 2.0$ (left) and $2.0 < |\Delta\eta| < 3.0$ (right).

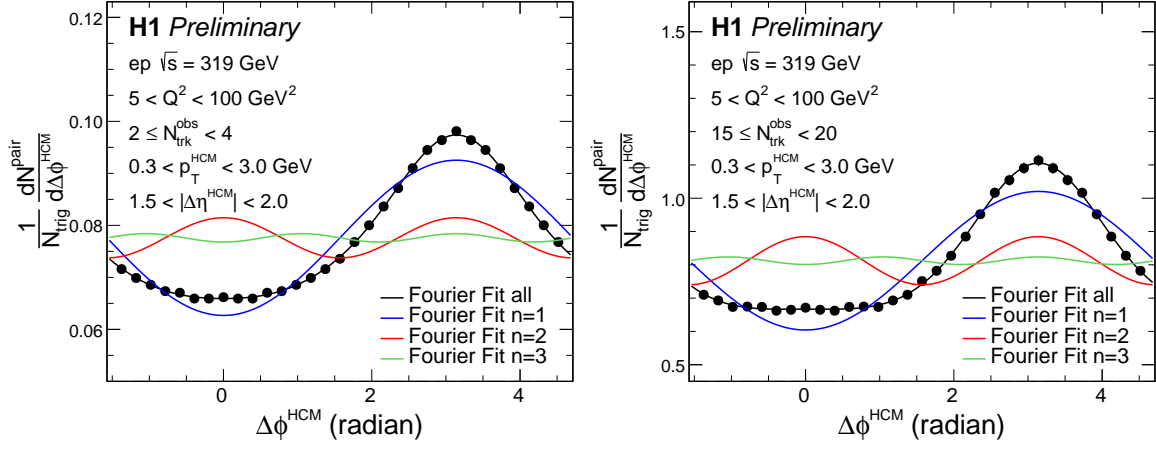


Figure 6: 1D $\Delta\phi^{HCM}$ correlation functions in H1 DIS events with $2 \leq N_{\text{trk}}^{\text{obs}} < 4$ (left) and $15 \leq N_{\text{trk}}^{\text{obs}} < 20$ (right) for charged particles with $0.3 < p_T^{HCM} < 3.0$ GeV and $1.5 < |\Delta\eta^{HCM}| < 2.0$. The solid lines show the Fourier decomposition fit.

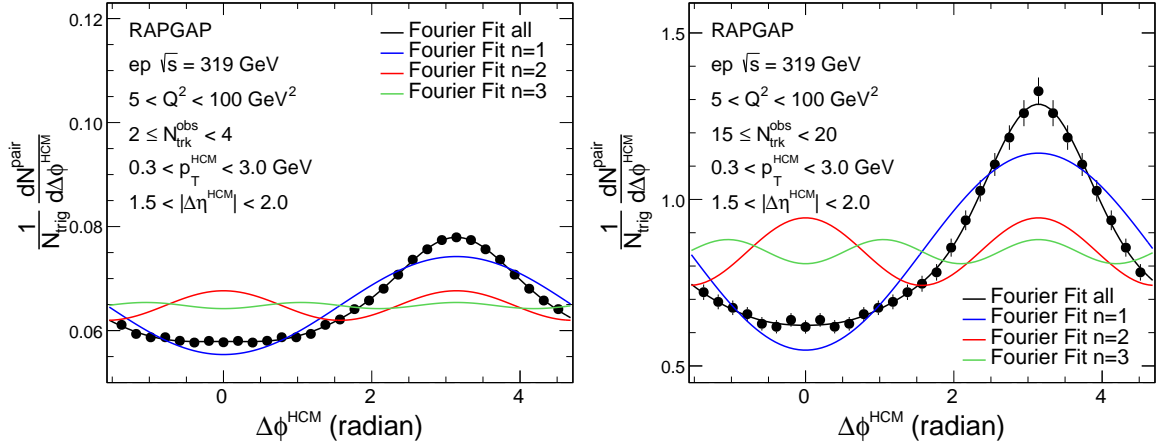


Figure 7: 1D $\Delta\phi^{HCM}$ correlation functions in RAPGAP DIS events with $2 \leq N_{\text{trk}}^{\text{obs}} < 4$ (left) and $15 \leq N_{\text{trk}}^{\text{obs}} < 20$ (right) for charged particles with $0.3 < p_T^{HCM} < 3.0$ GeV and $1.5 < |\Delta\eta^{HCM}| < 2.0$. The solid lines show the Fourier decomposition fit.

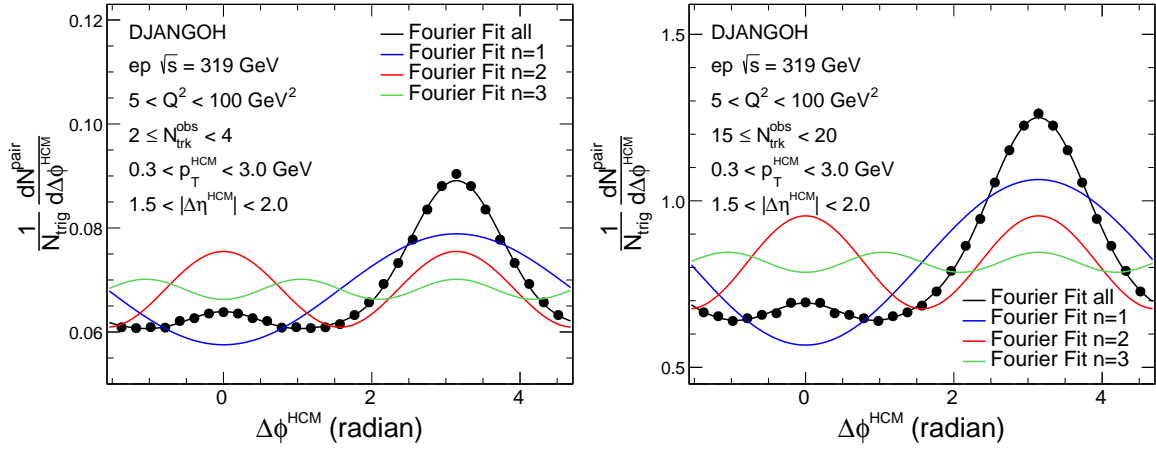


Figure 8: 1D $\Delta\phi^{HCM}$ correlation functions in DJANGO DIS events with $2 \leq N_{\text{trk}}^{\text{obs}} < 4$ (left) and $15 \leq N_{\text{trk}}^{\text{obs}} < 20$ (right) for charged particles with $0.3 < p_{\text{T}}^{HCM} < 3.0$ GeV and $1.5 < |\Delta\eta^{HCM}| < 2.0$. The solid lines show the Fourier decomposition fit.

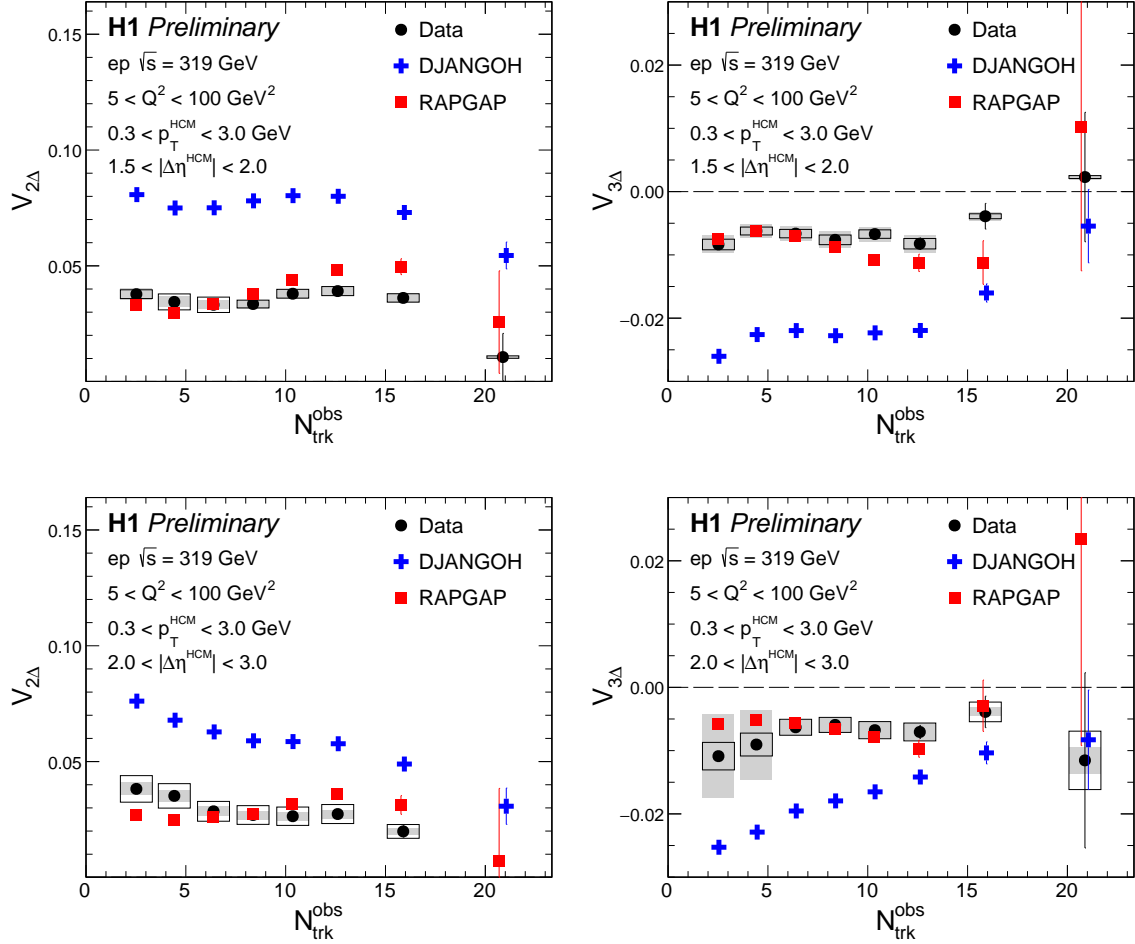


Figure 9: $V_{2\Delta}$ (left) and $V_{3\Delta}$ (right) as function of multiplicity in H1 DIS events for $1.5 < |\Delta\eta^{HCM}| < 2.0$ (top) and $2.0 < |\Delta\eta^{HCM}| < 3.0$ (bottom). Systematic uncertainties from Monte Carlo are shown as boxes. The other systematic uncertainties are shown as shaded areas.

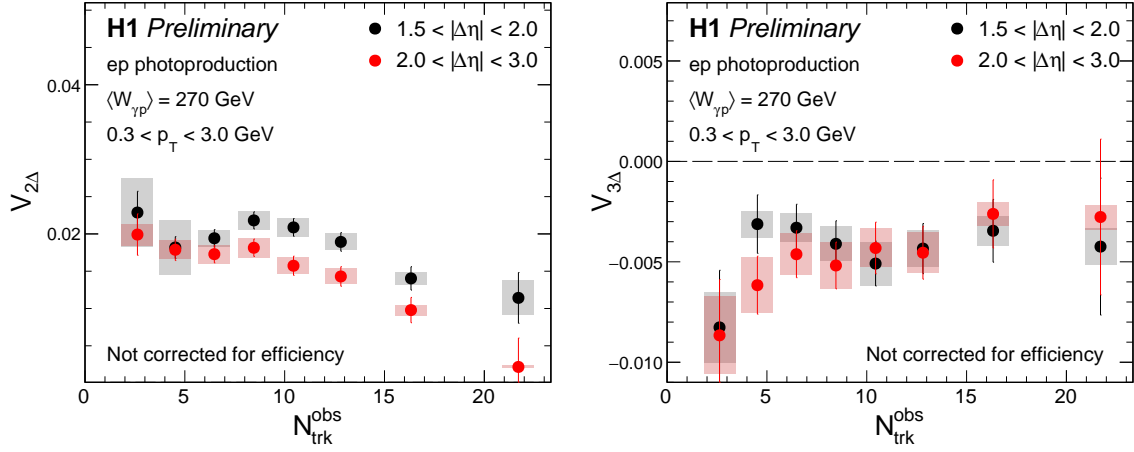


Figure 10: $V_{2\Delta}$ (left) and $V_{3\Delta}$ (right) as function of multiplicity in H1 photo-production events for $1.5 < |\Delta\eta| < 2.0$ and $2.0 < |\Delta\eta| < 3.0$. Systematic uncertainties are shown as shaded areas.

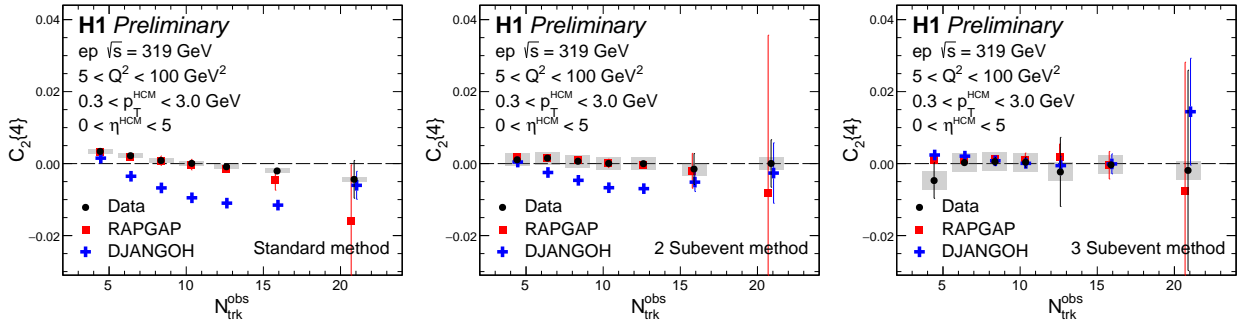


Figure 11: $C_2\{4\}$ as functions of multiplicity in H1 DIS events as well as in RAPGAP and DJANGO with the standard method (left), 2 subevent method (middle) and 3 subevent method (right). Systematic uncertainties are shown as shaded areas.

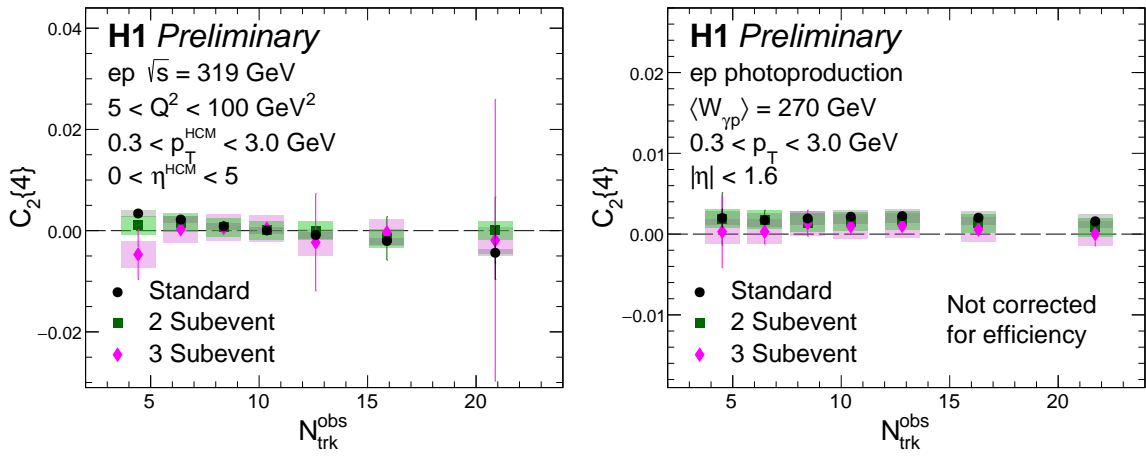


Figure 12: $C_2\{4\}$ as functions of multiplicity in H1 DIS (left) and photo-production (right) events with the standard method, 2 subevent method and 3 subevent method. Systematic uncertainties are shown as shaded areas.

References

- [1] S. Chatrchyan *et al.*, “Observation of long-range near-side angular correlations in pPb collisions at the LHC,” *Phys. Lett. B*, vol. 718, p. 795, 2013.
- [2] B. Abelev *et al.*, “Long-range angular correlations on the near and away side in pPb collisions at $\sqrt{s_{NN}} = 5.02$ TeV,” *Phys. Lett. B*, vol. 719, p. 29, 2013.
- [3] G. Aad *et al.*, “Observation of Associated Near-Side and Away-Side Long-Range Correlations in $\sqrt{s_{NN}}=5.02$ TeV Proton-Lead Collisions with the ATLAS Detector,” *Phys. Rev. Lett.*, vol. 110, no. 18, p. 182302, 2013.
- [4] R. Aaij *et al.*, “Measurements of long-range near-side angular correlations in $\sqrt{s_{NN}} = 5$ TeV proton-lead collisions in the forward region,” *Phys. Lett.*, vol. B762, pp. 473–483, 2016.
- [5] J.-Y. Ollitrault, “Anisotropy as a signature of transverse collective flow,” *Phys. Rev. D*, vol. 46, p. 229, 1992.
- [6] U. Heinz and R. Snellings, “Collective flow and viscosity in relativistic heavy-ion collisions,” *Ann. Rev. Nucl. Part. Sci.*, vol. 63, p. 123, 2013.
- [7] C. Gale, S. Jeon, and B. Schenke, “Hydrodynamic Modeling of Heavy-Ion Collisions,” *Int. J. Mod. Phys.*, vol. A28, p. 1340011, 2013.
- [8] S. Voloshin and Y. Zhang, “Flow study in relativistic nuclear collisions by Fourier expansion of azimuthal particle distributions,” *Z. Phys. C*, vol. 70, p. 665, 1996.
- [9] J. Jia, M. Zhou, and A. Trzupek, “Revealing long-range multiparticle collectivity in small collision systems via subevent cumulants,” *Physical Review C*, vol. 96, Sep 2017.
- [10] S. Chatrchyan *et al.*, “Long-range and short-range dihadron angular correlations in central PbPb collisions at $\sqrt{s_{NN}} = 2.76$ TeV,” *JHEP*, vol. 07, p. 076, 2011.
- [11] S. Chatrchyan *et al.*, “Centrality dependence of dihadron correlations and azimuthal anisotropy harmonics in PbPb collisions at $\sqrt{s_{NN}} = 2.76$ TeV,” *Eur. Phys. J. C*, vol. 72, p. 2012, 2012.
- [12] S. Chatrchyan *et al.*, “Multiplicity and transverse momentum dependence of two- and four-particle correlations in pPb and PbPb collisions,” *Phys. Lett. B*, vol. 724, p. 213, 2013.
- [13] V. Khachatryan *et al.*, “Observation of long-range near-side angular correlations in proton-proton collisions at the LHC,” *JHEP*, vol. 09, p. 091, 2010.
- [14] N. N. Ajitanand, J. M. Alexander, P. Chung, W. G. Holzmann, M. Issah, R. A. Lacey, A. Shevel, A. Taranenko, and P. Danielewicz, “Decomposition of harmonic and jet contributions to particle-pair correlations at ultrarelativistic energies,” *Physical Review C*, vol. 72, Jul 2005.

- [15] H. Jung, “Hard diffractive scattering in high-energy e p collisions and the Monte Carlo generator RAPGAP,” *Comput. Phys. Commun.*, vol. 86, pp. 147–161, 1995.
- [16] V. Gribov and L. Lipatov, “Deep inelastic e p scattering in perturbation theory,” *Sov. J. Nucl. Phys.*, vol. 15, pp. 438–450, 1972.
- [17] L. Lipatov, “The parton model and perturbation theory,” *Sov. J. Nucl. Phys.*, vol. 20, pp. 94–102, 1975.
- [18] G. Altarelli and G. Parisi, “Asymptotic Freedom in Parton Language,” *Nucl. Phys. B*, vol. 126, pp. 298–318, 1977.
- [19] Y. L. Dokshitzer, “Calculation of the Structure Functions for Deep Inelastic Scattering and e+ e- Annihilation by Perturbation Theory in Quantum Chromodynamics,” *Sov. Phys. JETP*, vol. 46, pp. 641–653, 1977.
- [20] J. Pumplin, D. Stump, J. Huston, H. Lai, P. M. Nadolsky, and W. Tung, “New generation of parton distributions with uncertainties from global QCD analysis,” *JHEP*, vol. 07, p. 012, 2002.
- [21] K. Charchula, G. Schuler, and H. Spiesberger, “Combined QED and QCD radiative effects in deep inelastic lepton - proton scattering: The Monte Carlo generator DJANGO6,” *Comput. Phys. Commun.*, vol. 81, pp. 381–402, 1994.
- [22] L. Lonnblad, “ARIADNE version 4: A Program for simulation of QCD cascades implementing the color dipole model,” *Comput. Phys. Commun.*, vol. 71, pp. 15–31, 1992.
- [23] E. A. Kuraev, L. N. Lipatov, and V. S. Fadin, “Multi - Reggeon Processes in the Yang-Mills Theory,” *Sov. Phys. JETP*, vol. 44, pp. 443–450, 1976.
- [24] E. Kuraev, L. Lipatov, and V. S. Fadin, “The Pommeranchuk Singularity in Nonabelian Gauge Theories,” *Sov. Phys. JETP*, vol. 45, pp. 199–204, 1977.
- [25] I. Balitsky and L. Lipatov, “The Pommeranchuk Singularity in Quantum Chromodynamics,” *Sov. J. Nucl. Phys.*, vol. 28, pp. 822–829, 1978.
- [26] L. Lonnblad, “Rapidity gaps and other final state properties in the color dipole model for deep inelastic scattering,” *Z. Phys. C*, vol. 65, pp. 285–292, 1995.
- [27] R. Brun, F. Bruyant, F. Carminati, S. Giani, M. Maire, A. McPherson, G. Patrick, and L. Urban, “GEANT Detector Description and Simulation Tool,” 10 1994.